

Università degli Studi di Napoli “Federico II”



**SCUOLA POLITECNICA E DELLE SCIENZE DI BASE
DIPARTIMENTO DI INGEGNERIA INDUSTRIALE**

CORSO DI LAUREA IN INGEGNERIA AEROSPAZIALE

CLASSE DELLE LAUREE IN INGEGNERIA INDUSTRIALE (L-9)

Elaborato di laurea in Meccanica del Volo

**An investigation on the lateral stability issues of the PROSIB 19-
pax aircraft model with OpenVSP**

Relatore:

Prof. Danilo Ciliberti

Candidato:

Schipani Angelo

Matr. N35003567

ANNO ACCADEMICO 2023 – 2024

Alla mia famiglia

E alla parte di me che non si è mai data per vinta.

Abstract

The purpose of this report is to analyze the issues related to the lateral stability of the PROSIB 19-passenger aircraft in the Wing-Body (WB) configuration, as the other components of the aircraft contribute negligibly to the case of interest. For the aerodynamic analysis, we used the VSPAERO software, after modelling was done in OpenVSP. Three different situations were examined: WB with flaps as sub-surfaces of the wing, WB with independent flaps from the main wing and attempts were made to reproduce the aircraft in the wind tunnel. The configurations were tested for different angles of attack (α) and sideslip angles (β), with the addition of flap deflection at 0, 15, and 30 degrees. Particular attention was given to the yaw (CM_z) and roll (CM_x) coefficients, which are indicators of lateral-directional stability. The collected data were finally compared with the data obtained experimentally in the wind tunnel.

Sommario

Lo scopo dell'elaborato è quello di andare ad analizzare le problematiche relative alla stabilità laterale del velivolo PROSIB 19 pax nella configurazione Wing-Body, dato che le altre componenti del velivolo contribuiscono in modo trascurabile al caso di interesse. Per l'analisi aerodinamica abbiamo utilizzato il software VSPAERO, dopo che la modellazione è stata effettuata su OpenVSP. Si sono prese in esame tre diverse situazioni: WB con flap come superfici ritagliate sull'ala, WB con flap indipendenti dall'ala principale e si è provato a riprodurre il velivolo in galleria del vento. Si sono testate le configurazioni per differenti angoli di attacco (α) e angoli di derapata (β), con aggiunta della deflessione dei flap di 0,15,30 gradi. Particolare attenzione è stata rivolta ai coefficienti di imbardata (CM_z) e rollio (CM_x), i quali sono indici della stabilità latero-direzionale. I dati collezionati, infine, sono stati confrontati con i dati ottenuti sperimentalmente nella galleria del vento.

Table of Contents

1.Introduction.....	5
1.1 Objectives	5
1.2 Layout of work.....	6
2.Vortex Lattice Method	6
2.1 VSPAERO	9
3. Geometric modelling	10
3.1 OpenVSP	10
3.2 Wing modelling.....	11
3.2.1 First modelling: subsurface technique	11
3.2.2 Second modelling: wing with slotted flaps	13
3.2.4 Third modelling: wind tunnel walls	17
4. Results and discussion.....	19
4.1 Sub Surface flaps setup	20
4.2 Slotted flaps setup	21
4.3 Comparing numerical results to experimental data	22
4.4 Simulation of the wind tunnel test section	25
5. Conclusion	28
References.....	29

List of figures

Figure 2.1-Vortex filament.....	9
Figure 3.1- Complete baseline model.....	10

Figure 3.2-3D scaled model	11
Figure 3.3-Base wing.	12
Figure 3.4-Modified main wing.....	13
Figure 3.5-Main wing's airfoil used images	14
Figure 3.6-Complete modeled wing with flap at 15°.	15
Figure 3.7- Flap at 15°	15
Figure 3.8-Complete wing with flaps at 30°.	16
Figure 3.9-Airfoils shape 30° flaps.....	17
Figure 3.10-First attempt.....	18
Figure 3.11-Second attempt.....	18
Figure 3.12-Measures test chambre(mm).	19
Figure 4.1-Wing Body configurations: left column rolling coefficient and right column yawing coefficient.	20
Figure 4.2-Wing Body configurations: left column rolling coefficient and right column yawing coefficient, all for independent flaps from main wing.	21
Figure 4.3-Comparing numerically and experimental data at $\alpha=0$	22
Figure 4.4-Comparing numerically and experimental data at $\alpha=5$	24
Figure 4.5-In reading order: $\beta=0^\circ$, $\beta=10^\circ$, $\beta=20^\circ$, $\beta=30^\circ$	26
Figure 4.6-Wind tunnel data analysis.	27

List of tables

Table 1-Used airfoil profile in first iteration.....	12
Table 2-Hub's coordinates	19

1.Introduction

The wind tunnel is the first experimental method developed to estimate the stability and control characteristics of an aircraft. The methods we know today, as described in manuals and notebooks, were developed from a large collection of wind tunnel data on the components of the tested models and their configurations. Nowadays, the wind tunnel is also used to present the tested cases to the research community to validate numerical methods, which can never completely replace the experimental approach but assist in the development and execution processes.

The aspect of the model that we investigated numerically was initially examined and preliminarily studied experimentally. This highlighted how a combined effect of lift-enhancing devices (flaps), sideslip angle, and angle of attack can be detrimental to lateral stability [1]. From other reports consulted, it was learned that, while keeping the aspect ratio constant and increasing the sweep angle, there is a significant reduction in roll damping at low lift coefficients only for high AR. Furthermore, the yawing moment and side force coefficient are directly proportional to the lift coefficient within a certain range for high sweep angles [2]. For wings without sweep angle, experimental data indicate that the rolling moment due to yaw is proportional to the lift coefficient up to the point of maximum lift [4].

1.1 Objectives

The purpose of the work carried out was to investigate the lateral stability of the Prosib 19-passenger aircraft, which initially exhibited lateral-directional instability both experimentally and when analyzed using the VSPAERO software. The objective of this study was to conduct a more detailed analysis of the Wing-Body configuration, carefully modified with OpenVSP, using VSPAERO, and to

determine if the results obtained reflected the wind tunnel data. All the data from the analyses conducted with VSPAERO were processed and plotted using Microsoft Excel. Finally, all the configurations tested were compared with the experimental data, and conclusions were drawn accordingly.

1.2 Layout of work

Chapter 2: This chapter provides a general overview of how the Vortex Lattice Method (VLM) works.

Chapter 3: This part of thesis explains the airplane's geometric modelling about the different configuration tested.

Chapter 4: This chapter illustrates collected data through the program, organization in graphs and tables, and comparisons with experimental data.

Chapter 5: Conclusion.

2.Vortex Lattice Method

These methods allow for quick and computationally efficient estimates of the aerodynamic forces and moments acting on an aircraft. The aircraft's geometry modeled by dividing the lifting surfaces, such as wings and tailplanes, into a network of elements. It is important to note that, despite the speed of this calculation method, it has limitations that do not allow for the analysis of overly complex structures. If we are dealing with a non-viscous and incompressible fluid, potential flow provides results under a wide range of conditions. This flow is accurately described by Laplace's equation. Irrotational flow is defined where vorticity is zero at every single point.

$$\xi = \nabla \times V = 0 \quad (1.1)$$

Considering the potential velocity, ϕ , it is obtained:

$$\nabla \times (\nabla\phi) = 0 \quad (1.2)$$

Combining the two equations written above, we have:

$$V = \nabla\phi \quad (1.3)$$

Furthermore, considering the conservation of mass and the incompressible flow, we obtain:

$$\nabla \cdot V = 0 \quad (1.4)$$

Combining the equations once again:

$$\nabla \cdot (\nabla\phi) = 0 \quad (1.5)$$

Or

$$\nabla^2\phi = 0 \quad (1.6)$$

The last obtained equation turns out to be, precisely, the Laplace equation. This method allows us to decompose the initial problem into more elementary

problems, which maintain the same characteristics. Considering the boundary conditions, this method linearizes and transforms the problem, leading to an approximation between pressure and velocity. If the approximation used to linearize the problem is valid, it implies that the thickness of the object being analyzed is not considered.

When considering the boundary condition of the wing, we find that the flow normal to its surface will be zero. This means that the sum of the normal component of the velocity induced by the vortices on the wing is zero. A solution of the Laplace equation is the singularity of the vortex point: Γ is referred to as the circulation force of the vortex. This has the same sign as the vorticity, being positive if in a clockwise direction. The mathematical description of the flow induced by this filament is given by the Biot-Savart law. It states that the increment of the velocity dV at a point P due to a segment of a vortex filament dl at a point q is:

$$dV_p = \frac{\Gamma}{4\pi} \cdot \frac{dl \cdot r_{pq}}{|r_{pq}|^3} \quad (1.7)$$

This can then be integrated over the entire length of the vortex filament to obtain the induced velocity in point P:

$$V_p = \frac{\Gamma}{4\pi} \cdot \int \frac{dl \cdot r_{pq}}{|r_{pq}|^3} \quad (1.8)$$

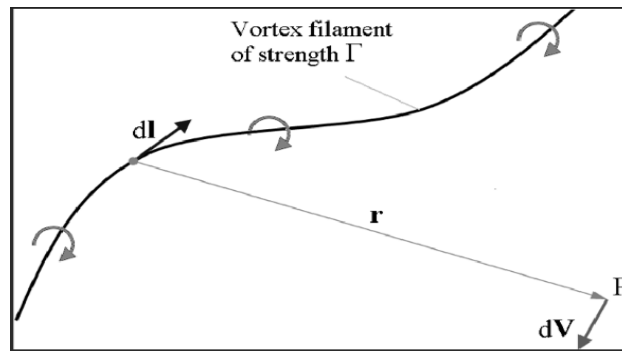


Figure 2.1-Vortex filament.

The surface of the model is divided into a finite number of panels (both transversely and longitudinally). Each of these panels contains a vortex, which has its own circulation and velocity. Therefore, to obtain the total aerodynamic force, it is necessary to sum the contributions from all the panels. The position of the vortex and that of a control point are important to satisfy the boundary condition of the surface. By applying principles such as the Kutta-Joukowski theorem, which relates the circulation around a lifting surface to the lift force, a system of linear equations is formed. These equations are solved iteratively to find the distribution of circulation and, consequently, the aerodynamic forces on the aircraft. Once the circulation distribution is determined, it is possible to calculate the aerodynamic coefficients such as lift, drag, and pitching moment.

2.1 VSPAERO

VSPAERO is an aerodynamic analysis module integrated into OpenVSP. It is a panel method tool that uses potential flow theory to calculate the aerodynamic properties of 3D models, such as lift, drag, and moments.

Based on panel theory and lifting-line techniques, VSPAERO is useful for the preliminary analysis of aircraft performance, allowing engineers to quickly assess the aerodynamic characteristics of complex configurations. It can handle both

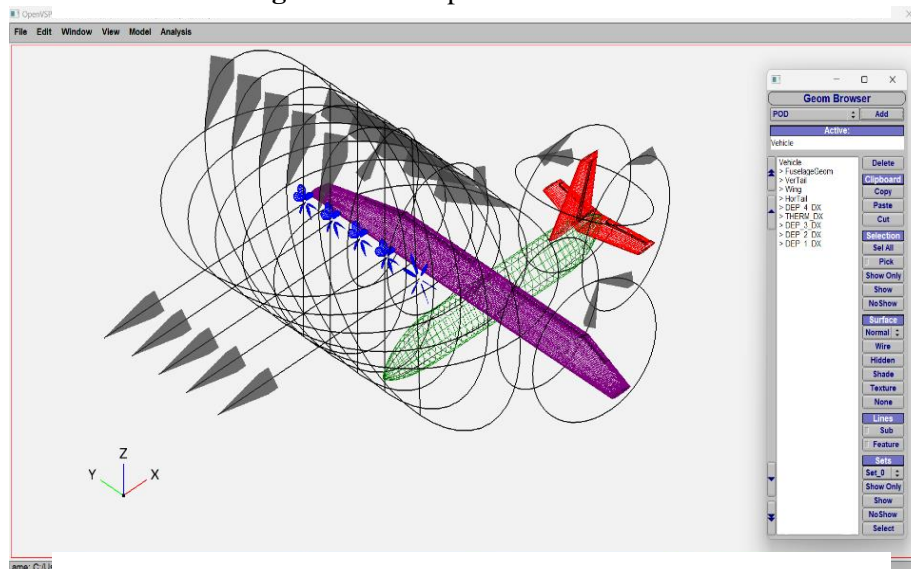
subsonic and supersonic flows and supports the analysis of unsteady aerodynamic forces.

3. Geometric modelling

3.1 OpenVSP

OpenVSP (Open Vehicle Sketch Pad) is an open-source software developed by NASA for the design and analysis of aerodynamic configurations of aircraft. It allows engineers and designers to create three-dimensional models of aircraft quickly and intuitively, using parametric geometric shapes. OpenVSP also enables the calculation of aerodynamic properties, such as lift and drag, through its integrated modules for preliminary analysis. As example can be see the full starting model of the thesis in figure 3.1.

Figure 3.1- Complete baseline model.



To illustrate how useful it can be, a photo of the 3D model of the aircraft is attached.

Figure 3.2-3D scaled model



3.2 Wing modelling

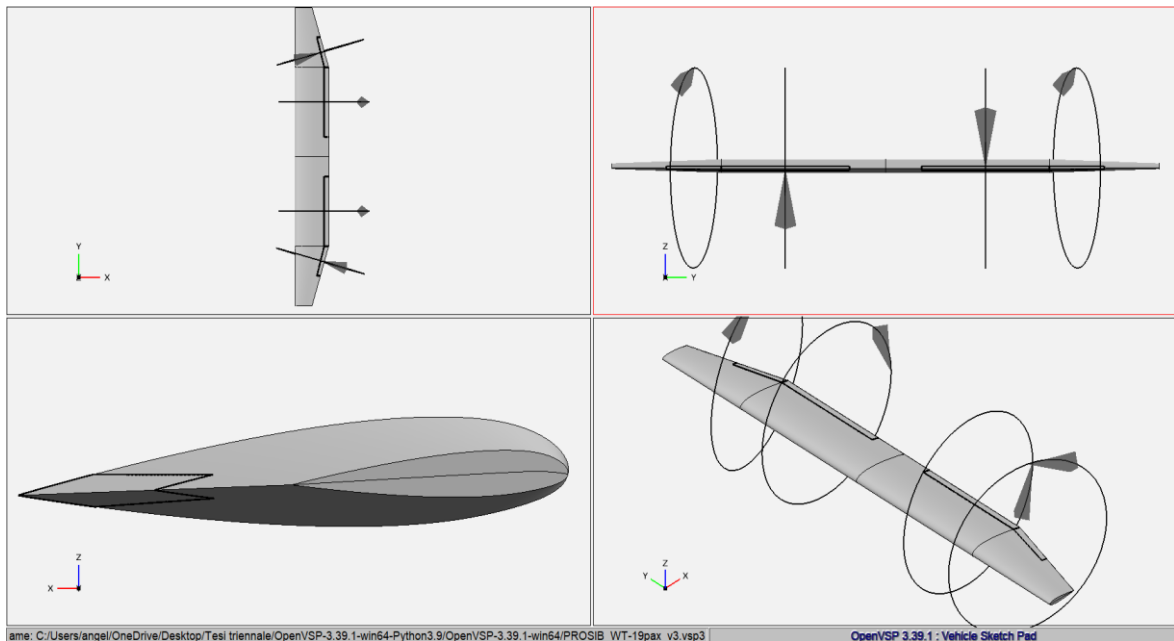
This paragraph is the first to address the actual modelling of the aircraft performed with OpenVSP.

As mentioned previously, we will not focus on the entire aircraft but rather on the modelling of the wings. This is because the case we want to study allows us to neglect the contributions of the tailplane and other disturbing elements. Consequently, the fuselage has also remained unchanged.

3.2.1 First modelling: subsurface technique

The wing from which we began the modelling and simultaneously the analyses is as follows.

Figure 3.3-Base wing.



In the fourth chapter, the data obtained from the analysis will be presented. This wing does not have independent flaps from the main surface; rather, they are drawn directly on the wing. This method is the quickest way to design the flaps, even though they do not accurately reflect reality, and it is the recommended method for studying the wing, given that OpenVSP has the limitation of not treating multiple wing surfaces as a single entity. Consequently, for the modelling, the function to divide the wing into sections was used, and in this case, two sections were utilized. The airfoil profiles used in the model are as follows:

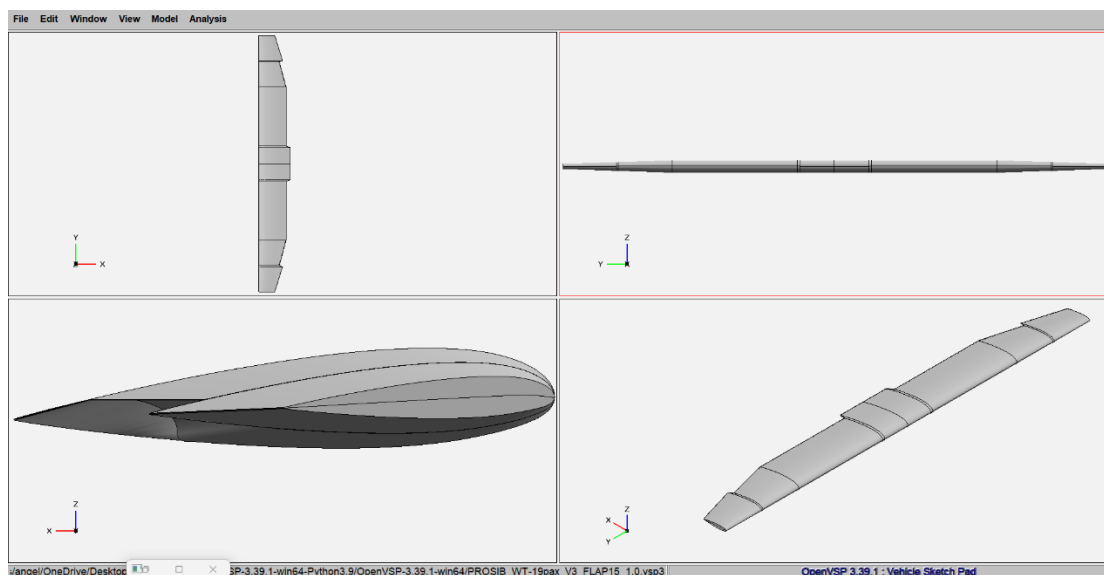
Root	Naca 23018
Kink	Naca 23018
Tip	Naca 23015

Table 1-Used airfoil profile in first iteration.

3.2.2 Second modelling: wing with slotted flaps

In the second case, we aimed to model the wing as realistically as possible, we first had to model the main section of the wing to accommodate the flaps. Below is an image to illustrate how the wing was modified.

Figure 3.4-Modified main wing



It should be noted that the wing in fig. 3.4 has multiple sections; six sections were used to refine the geometry as best as possible. This new wing was utilized for both the 15° and 30° cases, while it was unnecessary to analyse the 0° case, because given cove flap type the wing would resemble the initial one. The profile coordinates were obtained from the same 3D CAD used to create the model tested in the wind tunnel.

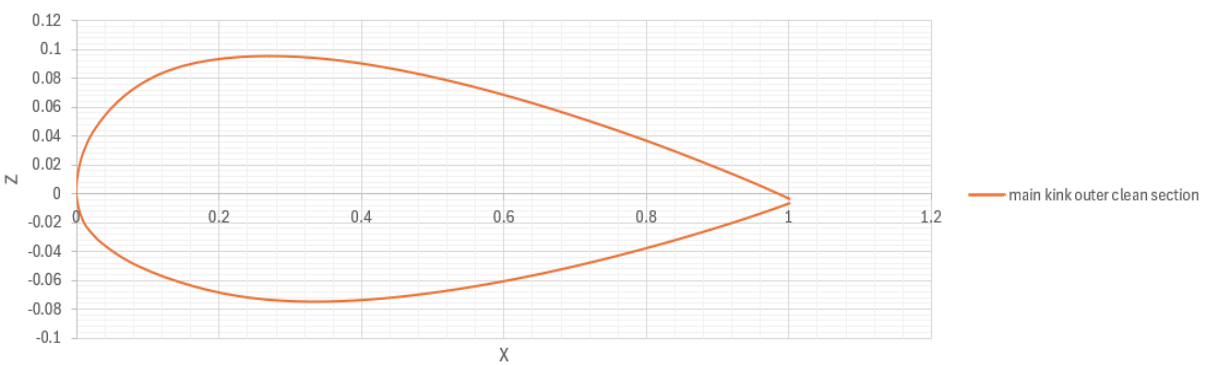
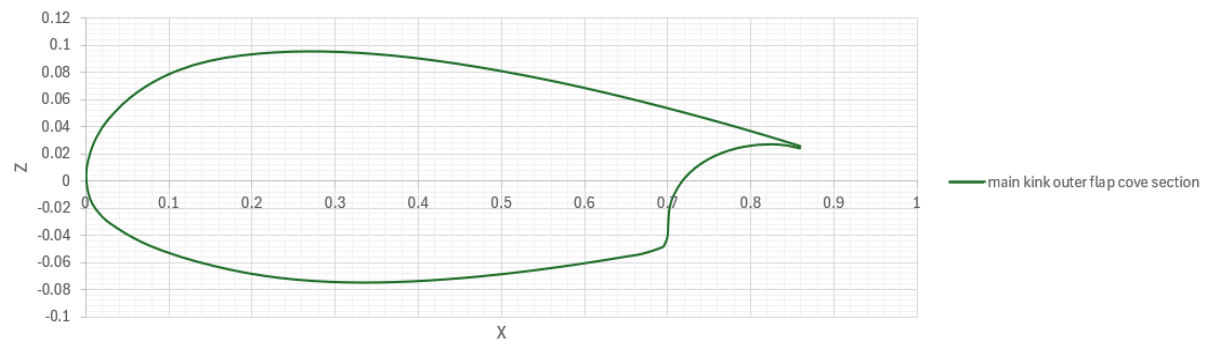
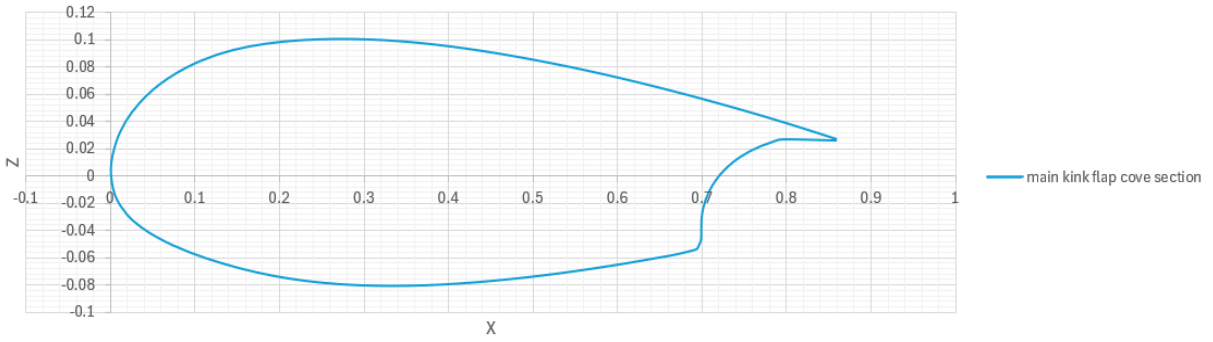
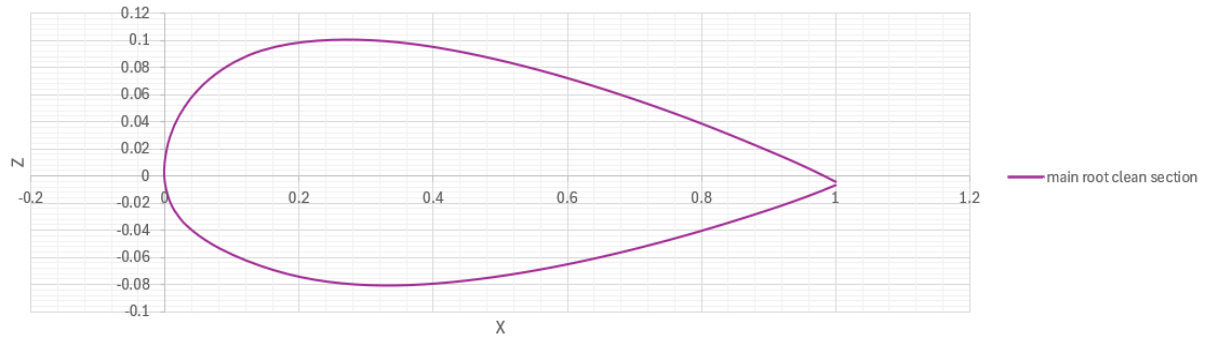
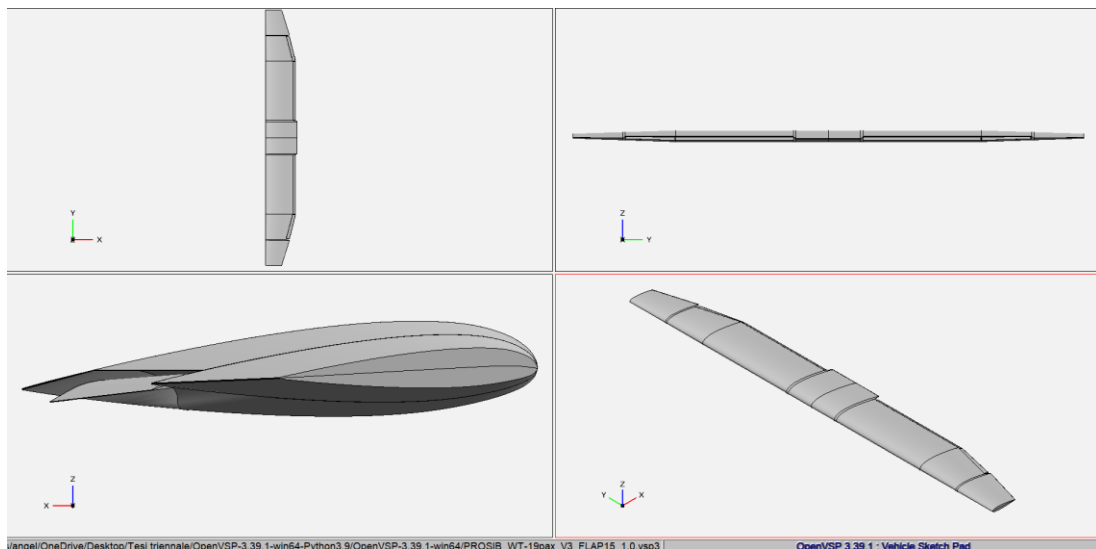


Figure 3.5-Main wing's airfoil used images

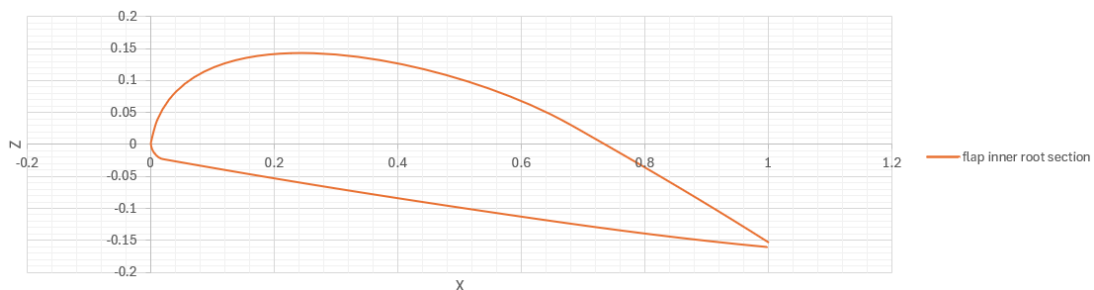
The flaps that are missing in Fig. 3.4 were added later. Since these surfaces do not have a specific command in OpenVSP for adding them, other than the one mentioned earlier, they were drawn under the "wing" command, thereby completing the geometry of the wing surface.

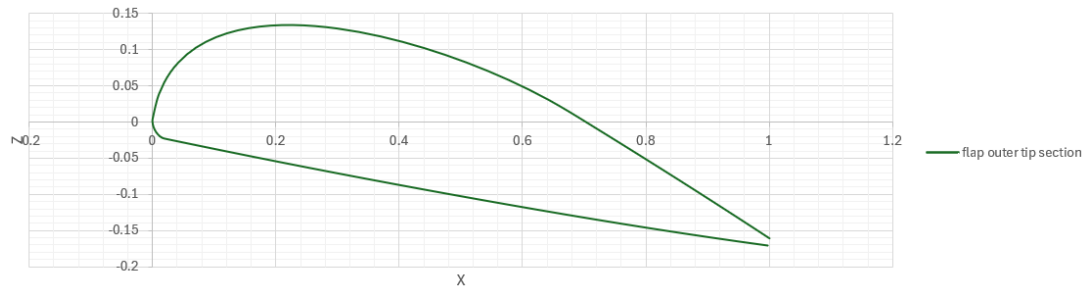
Figure 3.6-Complete modeled wing with flap at 15°.



Also in this case, the profile coordinates' flaps were imported from the same CAD 3D of the model. The profiles used are as follows:

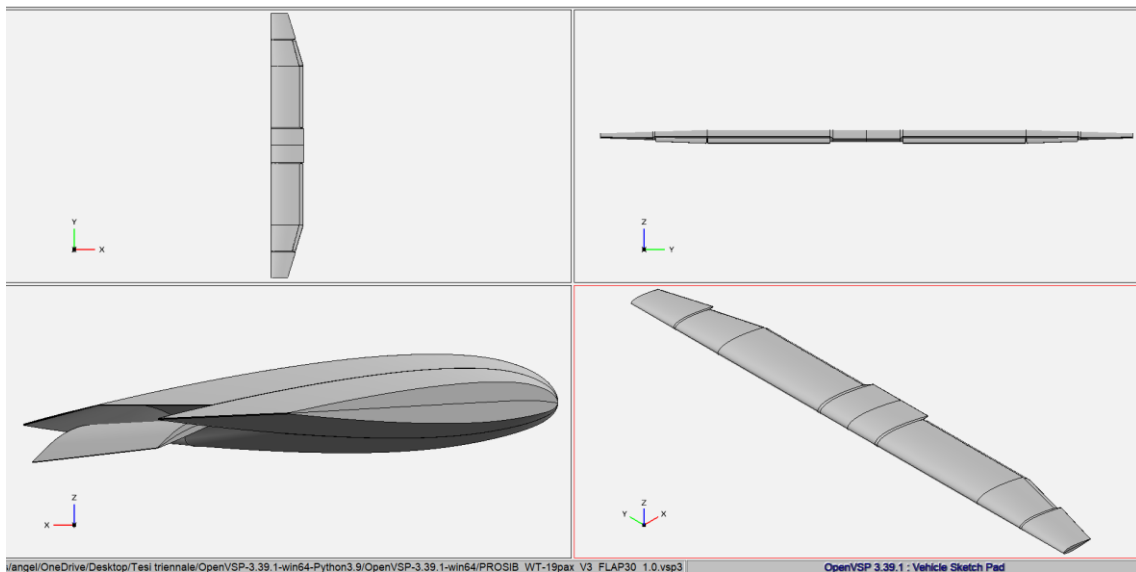
Figure 3.7- Flap at 15°





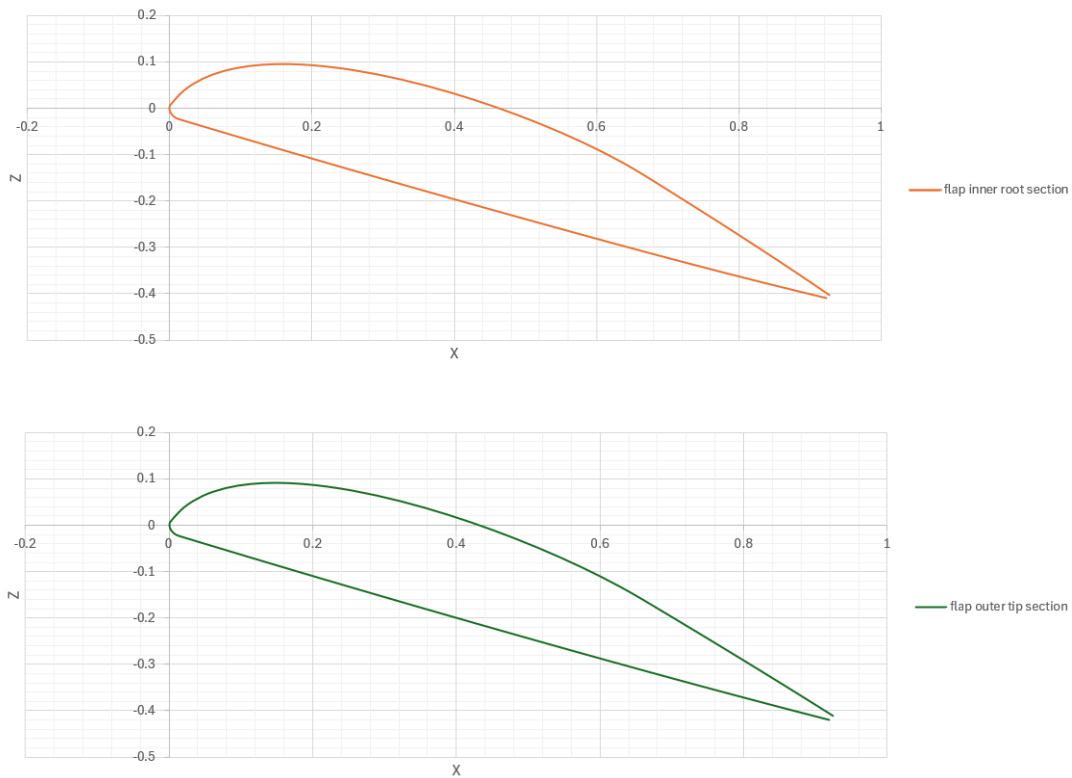
In this case, the same main wing represented in Fig. 3.4 was used. However, we changed the angle of the flaps to 30° , transitioning from the 15° flaps in Fig. 3.7 to the 30° flaps in Fig. 3.8.

Figure 3.8-Complete wing with flaps at 30° .



To draw them correctly, we followed the same procedure as for the previous flaps. The flaps used for the 30° configuration are as follows:

Figure 3.9-Airfoils shape 30° flaps.



3.2.4 Third modelling: wind tunnel walls

The final setup involves placing the aircraft inside the wind tunnel using OpenVSP and analyzing it with VSPAERO. To model the wind tunnel, two approaches were tested: one where the tunnel was represented as a duct, and another where it was modeled using wing-like surfaces. The first attempt did not produce any results because VSPAERO could not recognize the duct as an analyzable surface. The second approach proved useful for the analysis, as the software successfully detected the wing surfaces. Ultimately, this led to the following configurations.

Figure 3.10-First attempt.

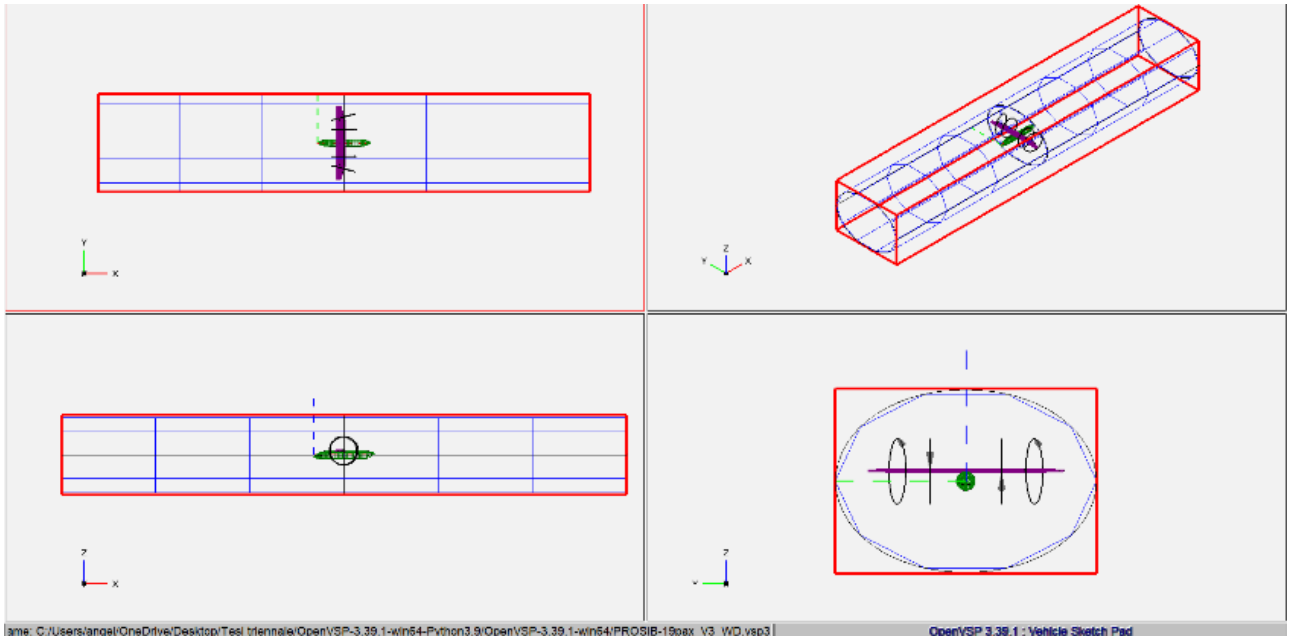
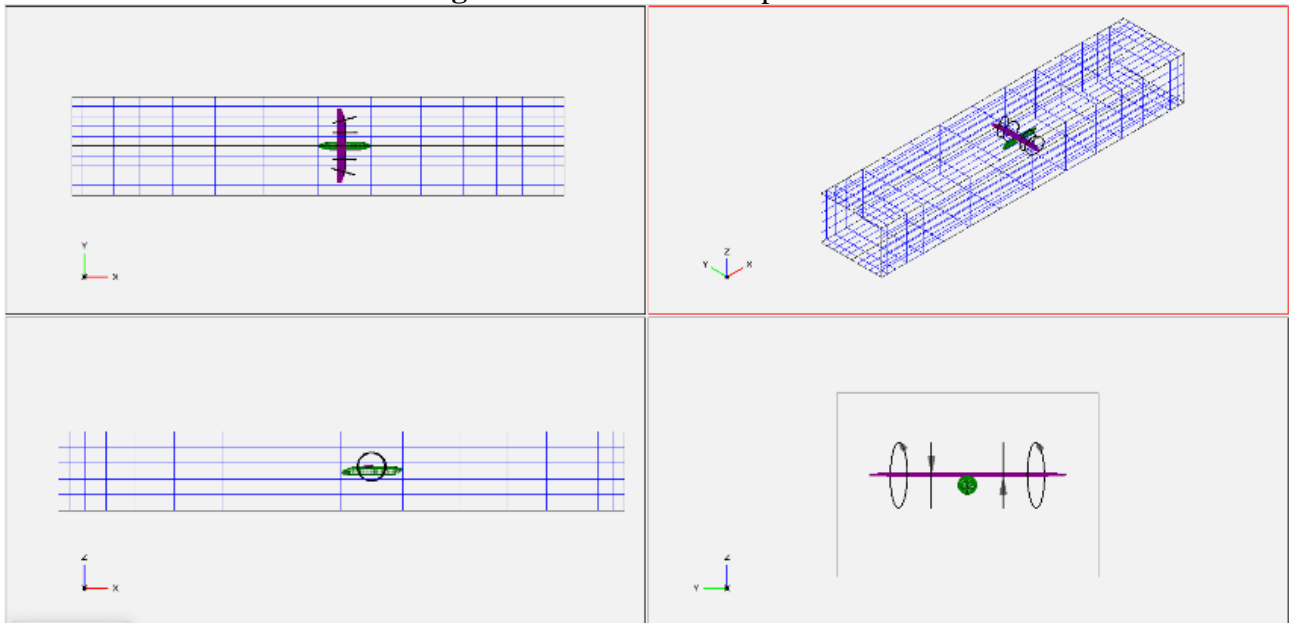
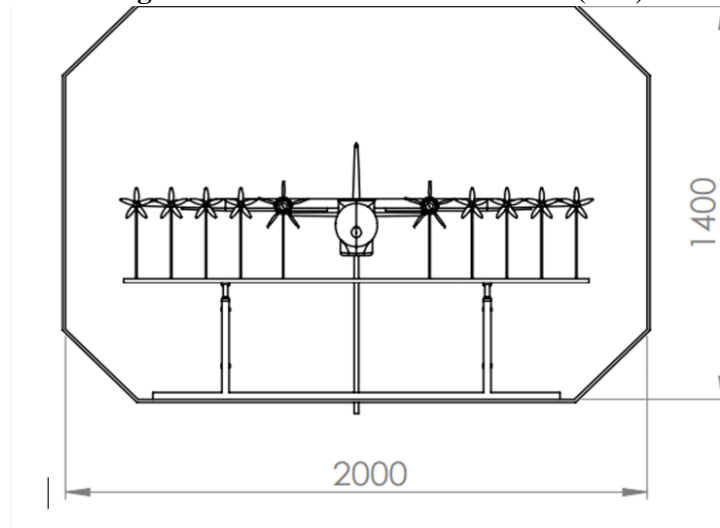


Figure 3.11-Second attempt.



The wind tunnel we referred to is the one used in [1], and the test chamber had the following dimensions.

Figure 3.12 – Measures test chambre(mm).



Unfortunately, due to the constraints imposed by OpenVSP, some simplifications had to be made, as shown in Fig. 3.11.

4. Results and discussion

The scope of the analysis on VSPAERO runs was to acquire the lateral-directional force and moments in variety conditions. The results are shown with standard aerodynamic coefficients of yawing moment(CM_z) and rolling moment(CM_x). To evaluate directional and lateral stabilities, the coefficients were estimated up to 30° of sideslip angle. The adopted hub for aerodynamic analysis has the following coordinates:

X	0.429
Y	0
Z	0

Table 2-Hub's coordinates(mm).

While the criteria for lateral-directional stability are:

$$C_{M_z} > 0, \quad C_{M_x} < 0$$

4.1 Sub Surface flaps setup

In this case, reference is made to Fig. 3.3, with the addition of the fuselage. The yaw moment coefficient is negative due to the absence of the tail plane. Meanwhile, the sign of the roll moment coefficient is positive for flap configurations at 15° and 30°, but not at 0°. Although the high-wing configuration should provide lateral stability.

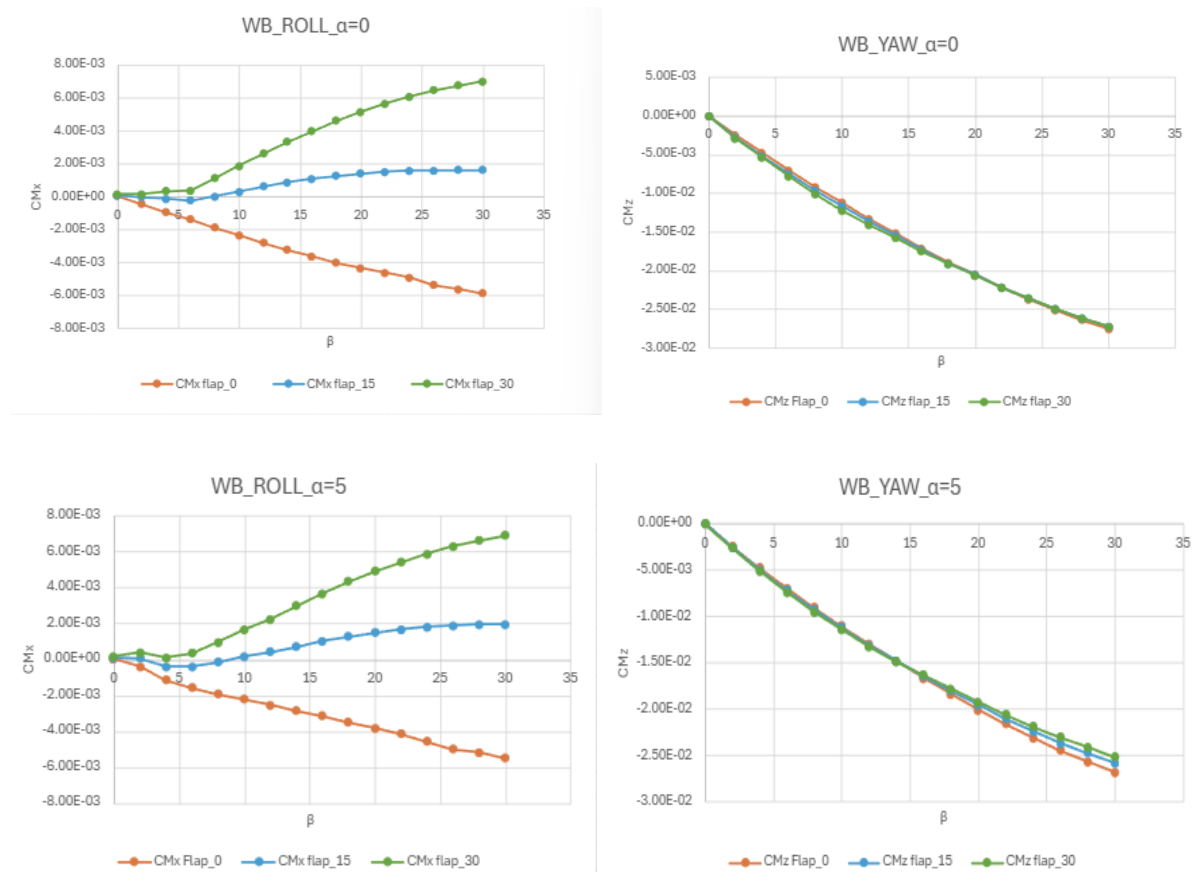


Figure 4.1 - Wing Body configurations: left column rolling coefficient and right column yawing coefficient.

Note that the graphs obtained by plotting the data extracted from the analyses are almost superimposable for the cases of alpha 0° and alpha 5°, for both roll and yaw.

4.2 Slotted flaps setup

As previously mentioned, in this case, only the 15° and 30° configurations were tested: refer to figures 3.6 and 3.8. When testing these configurations, note how the coefficients change; see figure 4.2.

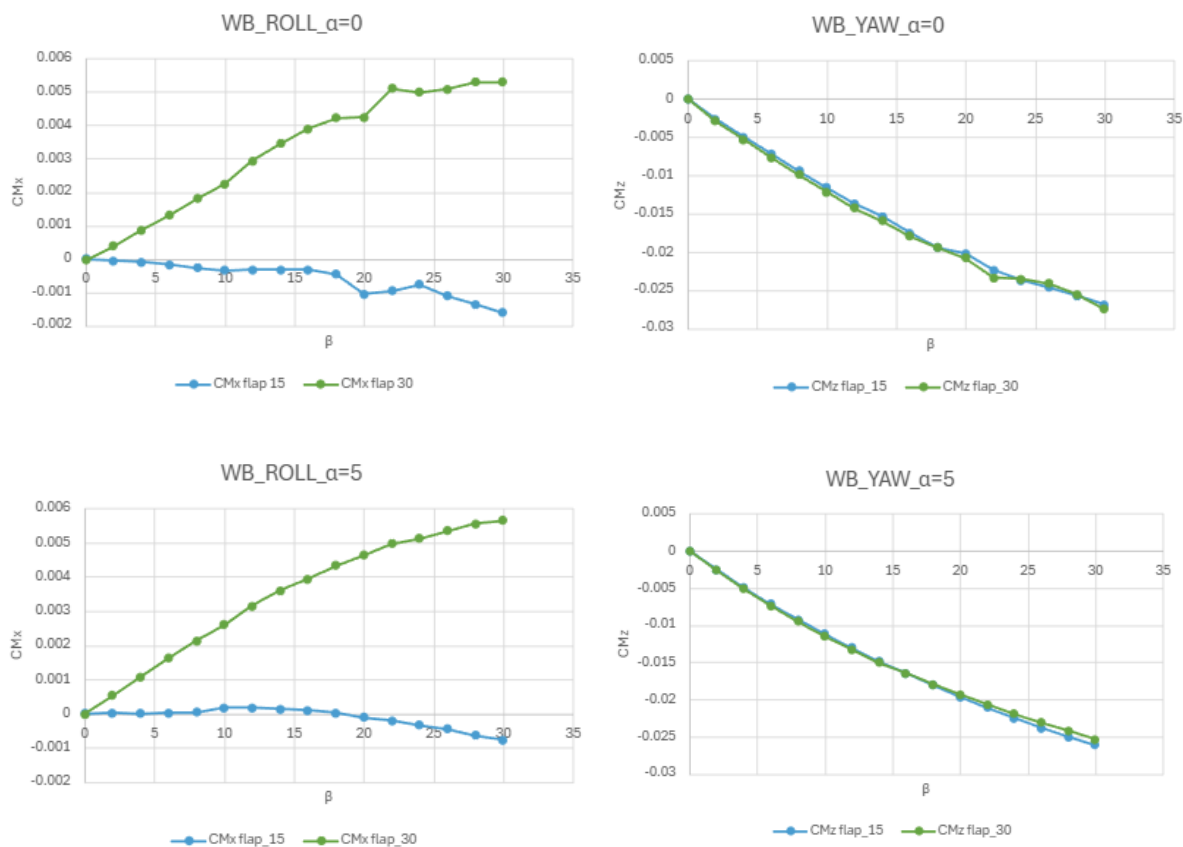


Figure 4.2- Wing Body configurations: left column rolling coefficient and right column yawing coefficient, all for independent flaps from main wing.

It is worth noting that, compared to the previous case, the rolling moment coefficient for the $\delta_f=15^\circ$ configuration gradually becomes negative, although with values close to 0, while for the $\delta_f=30^\circ$ configuration, it becomes larger in magnitude. As for the yawing moment coefficient. At $\delta_f=15^\circ$, the rolling moment coefficient remains within normal values. We still have not achieved lateral-directional stability.

4.3 Comparing numerical results to experimental data

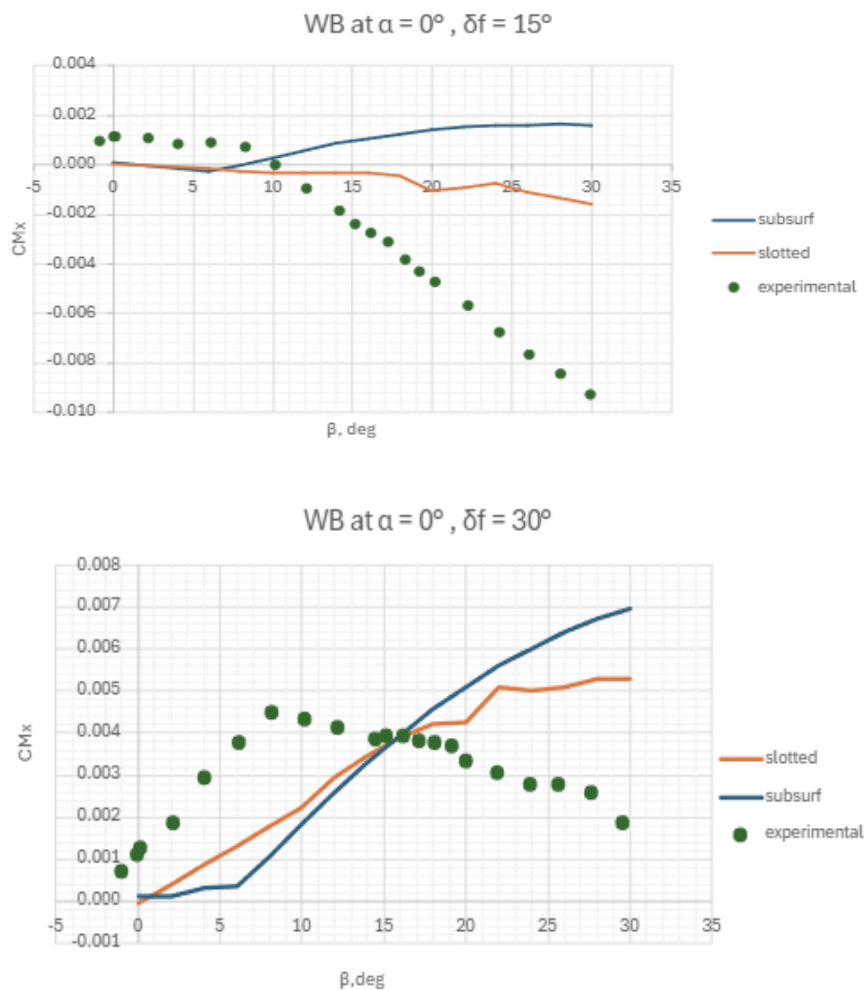
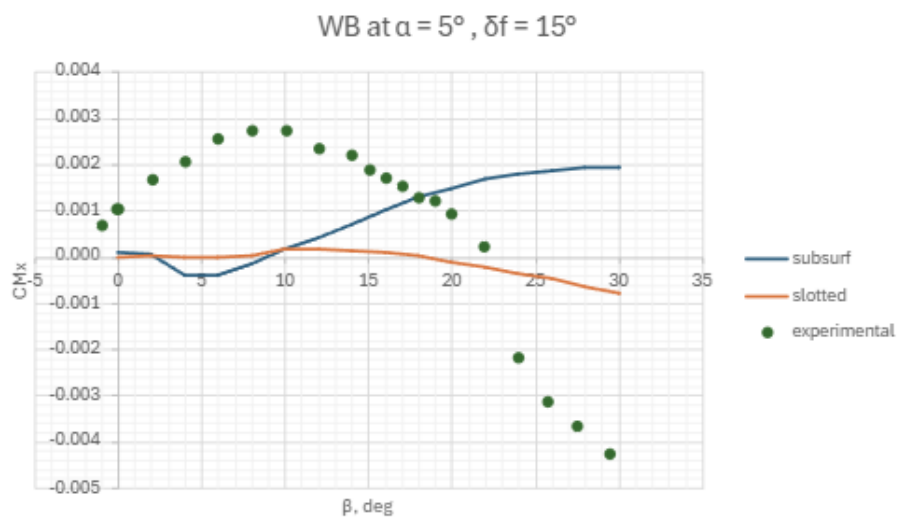


Figure 4.3-Comparing numerically and experimental data at $\alpha=0$.

At $\delta_f=15^\circ$ (First Graph): The experimental data shows a significantly greater negative roll response with increasing sideslip angle compared to both subsurface and slotted flap predictions.

At $\delta_f=30^\circ$ (Second Graph): The experimental data aligns more closely with the subsurface and slotted predictions, particularly at moderate sideslip angles. However, the subsurface configuration shows a strong positive roll response at larger sideslip angles, diverging more clearly from experimental data.

These graphs suggest that the flap configuration and deflection angle both impact the roll behavior under sideslip conditions. The subsurface configuration appears to produce a more consistent, increasing positive roll with sideslip angle, while the slotted configuration's effect is less pronounced or stabilizes. Experimental results, especially at lower flap deflection, indicate stronger sensitivity than the model predictions, particularly in terms of negative roll response.



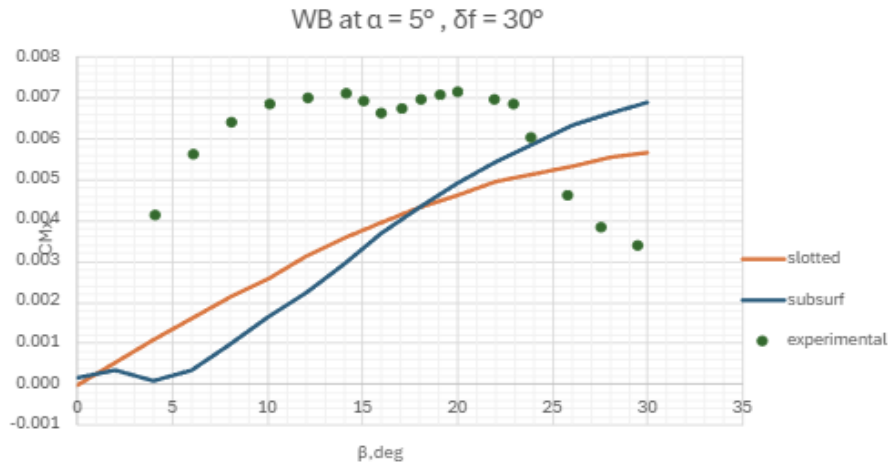


Figure 4.4-Comparing numerically and experimental data at $\alpha=5$

At $\delta_f=15^\circ$ (First Graph): The subsurface configuration generally produces a higher rolling moment coefficient than the slotted configuration, especially at higher sideslip angles. The experimental data initially match the subsurface trend but diverge significantly beyond $\beta=1,5^\circ$, indicating a reduction in the rolling moment coefficient at larger sideslip angles that neither configuration fully predicts.

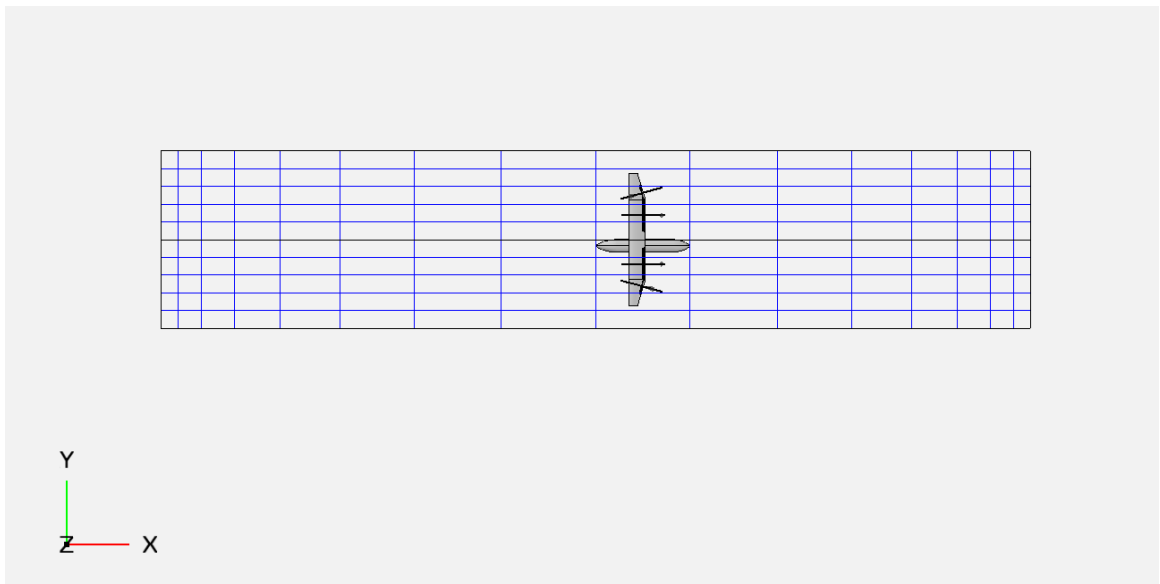
At $\delta_f=30^\circ$ (Second Graph): As the flap deflection angle δ_f increases, both flap configurations produce a higher rolling moment coefficient. The subsurface configuration tends to generate a higher rolling moment coefficient than the slotted configuration, particularly at larger sideslip angles. The experimental data closely follow the theoretical predictions at lower sideslip angles but diverge significantly beyond a certain angle.

In summary, increasing the flap deflection angle δ_f leads to a higher rolling moment coefficient for both configurations, with the subsurface configuration generally providing higher values, especially at larger sideslip angles. The experimental data show a similar trend to the theoretical curves at lower sideslip angles but diverge significantly at higher angles

4.4 Simulation of the wind tunnel test section

The following illustrates the data obtained in the third modelling phase, which aimed to investigate the feasibility of reproducing the aircraft in the wind tunnel using VSPAERO.

For the analyses, it was not possible to set a range of sideslip angle values; instead, the aircraft sideslip angle had to be modified directly in the design.



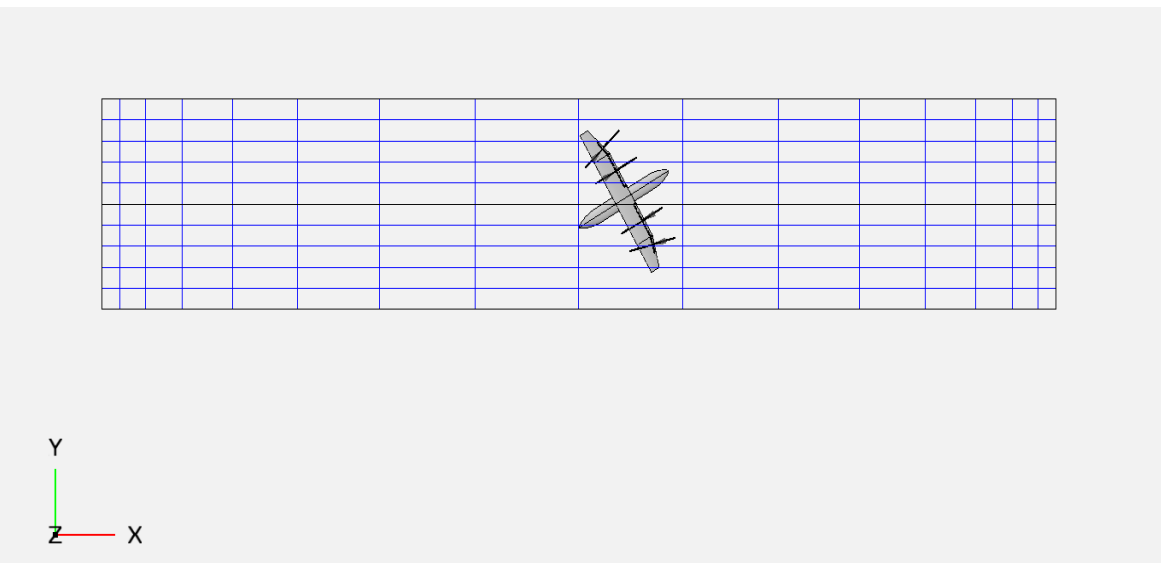
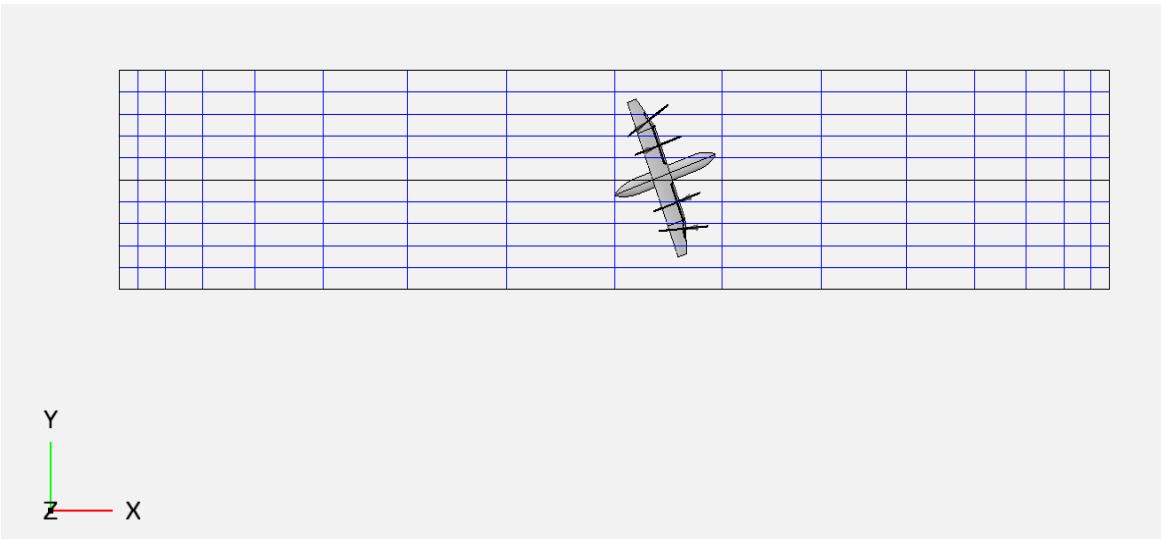
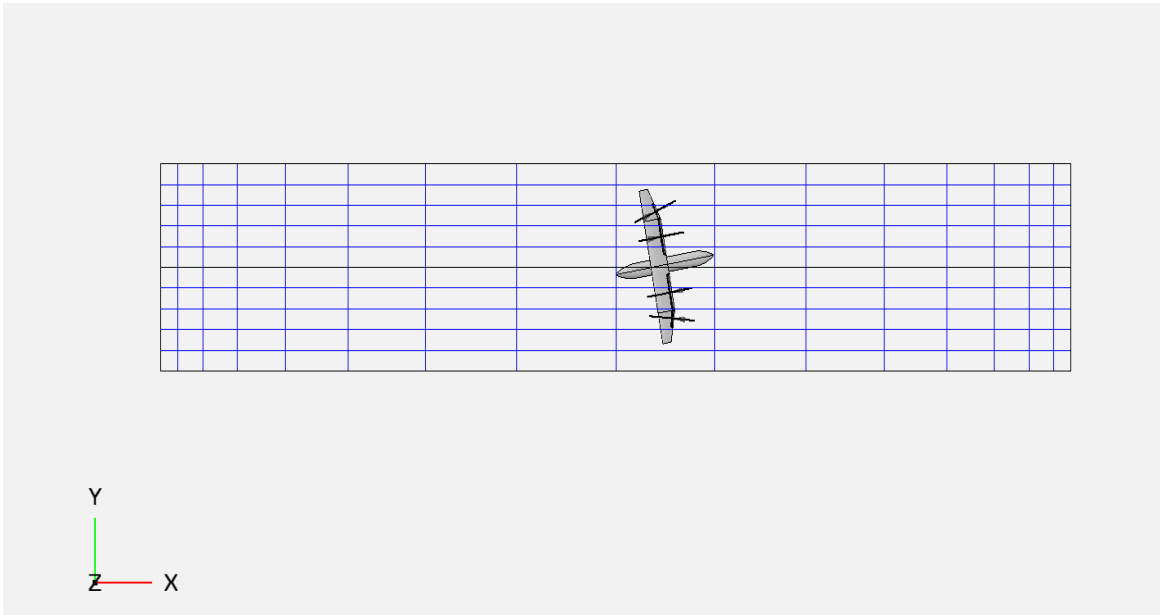
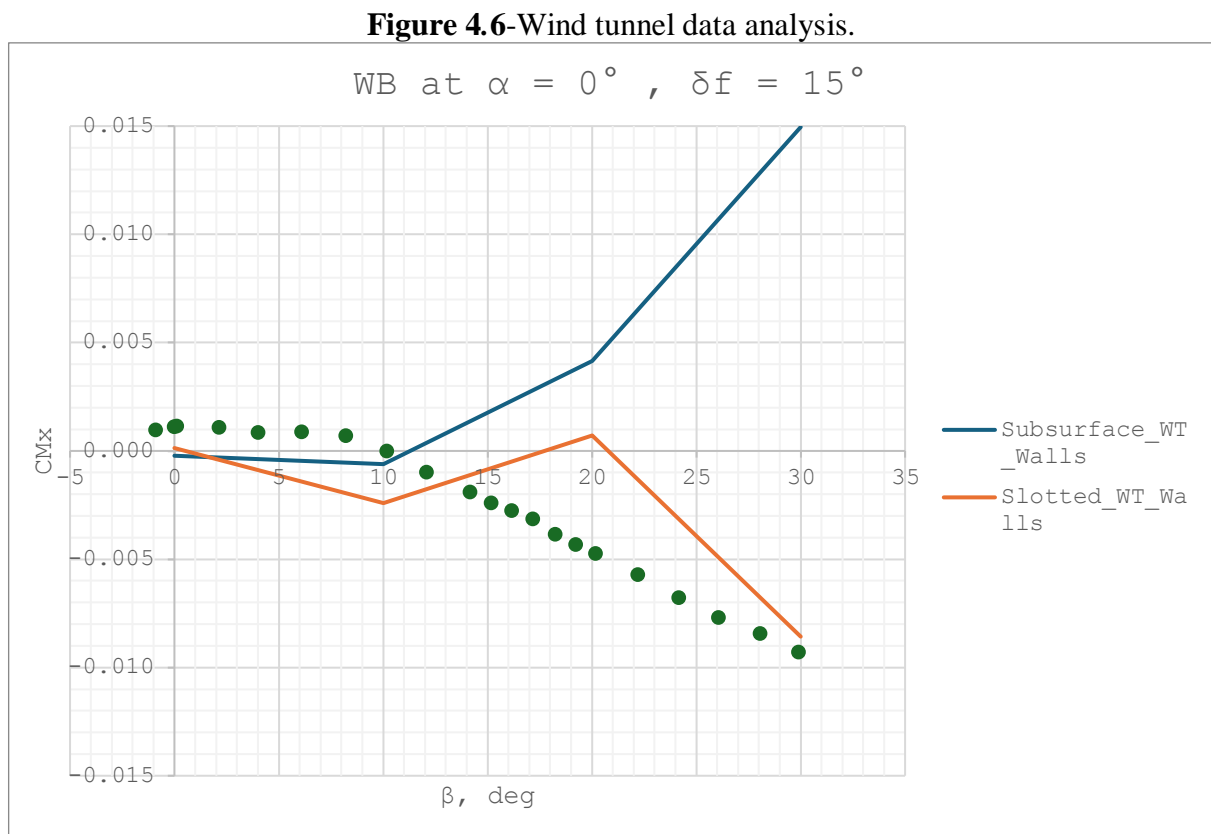


Figure 4.5-In reading order: $\beta=0^\circ$, $\beta=10^\circ$, $\beta=20^\circ$, $\beta=30^\circ$.

The images above show the aircraft in the baseline configuration, with the flaps as subsurface. The same procedure was also used in the case of slotted flaps.

The analyses are presented below.



Blue Line (Subsurface): The subsurface configuration shows an initial increase in the rolling moment coefficient at larger sideslip angles. Starting around $\beta=10^\circ$, the rolling moment coefficient begins to rise significantly and sharply increases past $\beta=25^\circ$, showing a positive trend.

Orange Line (Slotted): The slotted configuration produces a rolling moment coefficient that initially stays close to zero but then begins to decrease around $\beta=10^\circ$. After $\beta=15^\circ$, it shows a marked decline, reaching negative values and continuing downward past $\beta=25^\circ$.

Green Points (Experimental Data): The experimental data remain close to zero for lower sideslip angles, like both theoretical curves. After $\beta=10^\circ$, the experimental values begin to decline and become increasingly negative, aligning more closely with the trend of the slotted configuration as β increases, though the experimental results show a slightly less steep decline than the slotted curve.

Overall, the subsurface configuration yields a positive rolling moment coefficient at larger sideslip angles, while the slotted configuration results in a progressively negative coefficient. The numerical data of slotted configuration follow the experimental data trend, particularly after $\beta=10^\circ$ indicating a tendency toward negative rolling moments at higher sideslip angles.

5. Conclusion

The lateral-directional stability on the wing-body configuration of the PROSIB 19-passengers aircraft have been investigated. Referring to the data experimentally obtained from the wind tunnel, it is evident that the numerically derived values do not closely align with the experimental results, despite meticulous modeling of the aircraft. This confirms that OpenVSP and VSPAERO software best suited for linear behaviors, although the general trend of the rolling moment slope has been correctly followed.

References

- [1] Ciliberti, D., Nicolosi, F.: Lateral-directional wind tunnel tests of the PROSIB 19-pax aircraft model (2024).
- [2] Goodman, Fisher: Investigation at low speeds of the effect of aspect ratio and sweep on rolling stability derivatives of untampered wings.
- [3] Lichtenstein: Effect of high-lift devices on the low-speed static lateral and yawing stability characteristics of an untampered 45° sweptback wing, May 1952.
- [4] Goodman, Brewer: Investigation at low speeds of the effect of aspect ratio and sweep on static and yawing stability derivatives of untapered wings, August 1948.